

High-dimensional quantum key distribution with resource-efficient detection

MACIEJ OGRODNIK^{1,6,*}, ADAM WIDOMSKI^{1,6}, DAGMAR BRUSS², GIOVANNI CHESI³, FEDERICO GRASSELLI⁴, HERMANN KAMPERMANN², CHIARA MACCHIAVELLO³, NATHAN WALK⁵, NIKOLAI WYDERKA², AND MICHAŁ KARPIŃSKI¹

¹Faculty of Physics, University of Warsaw, Pasteura 5, 02-093 Warszawa, Poland

²Institut für Theoretische Physik III, Heinrich-Heine-Universität Düsseldorf, Universitätsstraße 1, D-40225 Düsseldorf, Germany,

³National Institute for Nuclear Physics, Sezione di Pavia, Via Agostino Bassi 6, 27100 Pavia, Italy

⁴Leonardo Innovation Labs – Quantum Technologies, Via Tiburtina km 12,400, 00131 Rome, Italy

⁵Dahlem Center for Complex Quantum Systems, Freie Universität Berlin, Arnimallee 14, D-14195 Berlin, Germany

⁶These authors contributed equally to this work.

*mm.ogrodnik@uw.edu.pl

Compiled December 24, 2024

High-dimensional encoding for quantum key distribution (QKD) enables increased achievable key rates and robustness as compared to the standard qubit-based systems. However, experimental implementations of such systems are more complicated, expensive, and require complex security analysis. In this work we present a proof of principle high-dimensional time-phase BB84 QKD experiment using only one single-photon detector per measurement basis. We employ the temporal Talbot effect to detect QKD symbols in the control basis, and show experimentally-obtained values for the two-dimensional and four-dimensional case. We present a comparison of the secret key rates obtained from two different security proofs to display security issues stemming from asymmetric detection efficiencies in the two bases. Our results contribute to the discussion of the benefits of high-dimensional encoding and highlight the impact of security analysis on the achievable QKD performance.

<http://dx.doi.org/10.1364/ao.XX.XXXXXX>

1. INTRODUCTION

Advancements in quantum computing pose a significant threat to the security of communication systems. Quantum key distribution (QKD) provides protocols with provable security under minimal assumptions on the adversary, in contrast to classical cryptography solutions. The security of practical QKD systems relies on how well the system corresponds to the theoretical model of a QKD protocol [1]. Different physical realizations of QKD protocols come from practical considerations such as cost, speed or complexity of the system. Many systems use qubits (states in a 2-dimensional Hilbert space) which carry one bit of information per photon [2–4]. With d -dimensional quantum states (qudits), one can increase the bits of information per symbol to $\log_2(d)$ bits [5]. Qudits enable tolerating higher quantum bit error rates (QBERs) present in quantum communication [6, 7] and overcoming problems related to saturation of the receiver’s single-photon detectors [8]. As a result, higher secret key rate values can be achieved in comparison to the binary encoding ($d = 2$) scenario [5, 9]. Constructing a high-dimensional

QKD system requires the ability to generate and detect high-dimensional quantum states and their superpositions in the key generation and control bases, which comes at a cost of higher complexity as compared to qubit systems. Various photons’ degrees of freedom were used in high-dimensional QKD experiments. Experiments using OAM [10–12], polarization [13], or spectro-temporal degree of freedom were successfully performed over fiber [14, 15] and free-space [16] quantum channels.

Most security proofs for QKD are based on abstract quantum states, independent of their physical realization. To apply these proofs to real-world systems, it is necessary to ensure that the setup reliably prepares and measures quantum states according to the assumptions of the proof, even in the presence of adversarial manipulations. The time-phase variant of the BB84 protocol with weak coherent pulses and the decoy state method is a well-researched encoding scheme [17]. Typically, Franson interferometers [14, 18] are employed to detect phases between light pulses. However, a single interferometer measures the phase between only two time bins. To detect high-dimensional states

such interferometers have to be nested [19, 20], which implies higher complexity, cost, and losses. The probability to detect a qudit with a passive interferometer tree is scaled by the $1/d$ factor due to the increased number of paths the superposition may take [19, 21]. The alternative approach of active switching enables more efficient detection of time-bin superposition, at the cost of significantly increased experimental complexity [22, 23].

Alternatively, temporal mode superpositions were measured by means of the optically nonlinear quantum pulse gate [24–26]. However, these methods necessitate active spectral modification, involving complex setups and ultrashort laser pulses at the detection stage. In principle, tailored time-frequency basis transformations could be used [27–29], but their efficient experimental implementation is still to be developed. Additionally, such implementations often result in a mismatch between measurement probability in the two bases. This inequality should be considered in the security proof and relevant key rate calculations. Several attempts to incorporate this effect have been made [30–35], yet it is a major challenge to fully model the real operation of physical devices such that all side-channel attacks can be avoided.

In this work we present an alternative scheme for high-dimensional QKD using time-phase encoding and spectral-temporal decoding, which allows using the same passive receiver architecture regardless of the dimension. We use the temporal Talbot effect [21, 36, 37], to discriminate qudits in the control basis. Our experimentally simple method only requires a dispersive medium and a single time-correlated single photon counter. Qudit exchange was tested in two and four-dimensional scenario for fiber-based quantum channel attenuations spanning up to 27.24 dB using the same setup. The measurements were conducted utilizing in-lab fibers as well as urban dark-fiber infrastructure of the University of Warsaw.

In addition to the novel protocol implementation and its tests, we present a theoretical comparison of the asymptotic secret key rates for different dimensions considering experimentally-obtained parameters using two different security proofs. In particular, we compare the key rates obtained with the standard BB84 protocol, which assumes that the detection probability at Bob is independent of the measurement basis, and with a recent security proof by F. Grasselli *et al.* [38], where the asymmetric detection efficiency in the two bases is accounted for.

The manuscript is organized as follows: in the “Protocol” section we describe our encoding scheme, detection method and show the formula for the key rate. In the “Experiment” section we describe the setup, including the locations of fiber network nodes, and data acquisition methods. The results, QBER, and theoretical key rate analysis using the standard high-dimensional BB84 approach are contained in the “Results and discussion” section. We proceed with a short description of vulnerabilities in the “Security discussion” section. We then apply the new security proof in the “Tunable beam splitter protocol” section to highlight the differences stemming from security analysis, and finally conclude and compare the results in the “Conclusion” section.

2. PROTOCOL

Let us consider optical pulses in d orthogonal time bins $|t_0\rangle, |t_1\rangle, \dots, |t_{d-1}\rangle$ forming the Z (key generation) basis, and d superpositions of those states that form a discrete Fourier transform of the Z basis [39], comprising the X (control) basis:

$$|f_n\rangle = \frac{1}{\sqrt{d}} \sum_{m=0}^{d-1} e^{-\frac{2\pi i n m}{d}} |t_m\rangle. \quad (1)$$

Then, the two bases are mutually unbiased and satisfy the relation [40]:

$$|\langle f_n | t_m \rangle|^2 = \frac{1}{d} \quad \forall m, n. \quad (2)$$

We use those bases to realize the d -dimensional BB84 protocol with information encoded in the time-phase degrees of freedom. We utilize the two-decoy scheme to avoid photon-number splitting attacks.

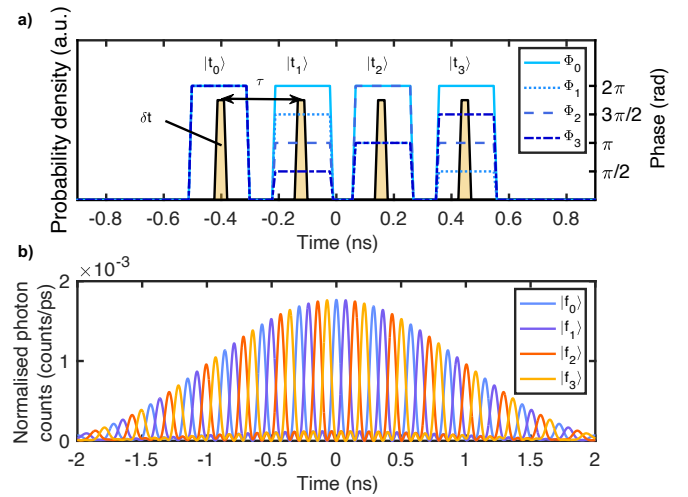


Fig. 1. State preparation. a) Generating high-dimensional states. The symbols were approximately rectangular optical pulses attenuated to single-photon level, 46 ps wide, and separated by 284 ps. Electrical signals used to impose phase modulation were 150 ps wide, and their amplitude was adjusted with respect to the half-wave voltage of the employed phase modulator, cf. Fig. 2. b) Simulated temporal Talbot effect on time of arrival probability density functions of high-dimensional states generated as in a).

Fig. 1a) depicts the temporal profiles of optical and electrical signals used for generating the quantum states used in this work for the $d = 2$ and $d = 4$ case. We adjust the separation between the components of the superposition τ and their width δt such that detection using the temporal Talbot effect is possible. The measurement is realized by means of temporal self-imaging using a dispersive medium with a specific group delay dispersion (GDD), further called the Talbot GDD [37]. The temporal location of the self-images depends on the relative phases of superposition’s components, which makes different superpositions distinguishable [21]. Therefore, information in both the bases is measured only in the time domain. The temporal Talbot condition imposes the following relation between the pulse separation (τ) and GDD (β_2):

$$\tau = \sqrt{\frac{2\pi\beta_2}{s}}, \quad s = 1, 2, \dots \quad (3)$$

By employing the temporal Talbot effect we are able to construct an all-fiber detection system with one single-photon detector per measurement basis, resulting in a very simple setup. We show how the X -basis QBER related to our method scales with the dimension in the “Results and Discussion” section.

The asymptotic secret key rate for a d -dimensional BB84 protocol in the 2-decoy variant is given by [38]:

$$r_{\text{BB84}} = p_Z^2 \sum_{j=1}^3 p_{\mu_j} \left\{ e^{-\mu_j} Y_0^Z \log_2 d + e^{-\mu_j} \mu_j Y_1^Z [\log_2 d - u(\overline{e_{X,1}})] - G_{\mu_j}^Z u(Q_{Z,\mu_j}) \right\}, \quad (4)$$

where p_Z is the probability to prepare (measure) in the Z basis, while the X basis is chosen with probability $1 - p_Z$. Alice selects the symbol $j \in \{0, \dots, d-1\}$ ($k \in \{0, \dots, d-1\}$) and intensity $\mu_j \in \mathcal{S} := \{\mu_1, \mu_2, \mu_3\}$ with probabilities p_{μ_1} , p_{μ_2} and $p_{\mu_3} = 1 - p_{\mu_1} - p_{\mu_2}$. An upper bound on the bit error rate in the control basis is denoted as $\overline{e_{X,1}}$, Y_0^Z and Y_1^Z are 0 and 1-photon yields in the Z-basis, $G_{\mu_j}^Z$ and Q_{Z,μ_j} are respectively the gain and QBER corresponding to a state with μ_j mean photon number.

The function $u(x)$ appearing in Eq. (4) is defined as:

$$u(x) = \begin{cases} h(x) + x \log_2(d-1) & \text{if } x \in \left(0, 1 - \frac{1}{d}\right) \\ \log_2 d & \text{if } x \in \left[1 - \frac{1}{d}, 1\right), \end{cases} \quad (5)$$

with $h(x) = -x \log_2 x - (1-x) \log_2(1-x)$ the binary entropy.

3. EXPERIMENT

The schematic of the experimental setup is presented in Fig. 2.

A distributed-feedback (DFB) laser operating at the telecommunication wavelength of 1560 nm in the continuous wave (CW) mode was used as the main optical source. We amplified the optical signal with an erbium-doped fiber amplifier (EDFA, Pritel, HPP-PMFA-22-10) and employed a bandpass spectral filter to reduce the noise and provide sufficient power for a feedback loop, discussed later. The optical signals and decoy states for both the bases were generated by means of cascaded fast amplitude electro-optic modulation with a pair of Mach-Zehnder modulators (MZM, Thorlabs, LNA6213). We biased both the MZMs for extinction with the direct current (DC) voltage from a stable power supply (Keysight, E36313A) using the feedback loop consisting of a 90:10 fiber optic beam splitter and a power meter (Thorlabs, PM400) (not shown in Fig. 2). The second modulator was biased with another feedback loop comprising a separate CW laser for calibration, a power meter, an isolator, and a switch used to cut off the calibration laser for the time of key distribution. We controlled the mean photon numbers by driving both the modulators (μ_1), one modulator (μ_2), or none of them (μ_3). The mean photon numbers for in-lab and infrastructural experiments were equal to $\mu_1 = 0.06$, $\mu_2 = 6.59 \cdot 10^{-4}$, $\mu_3 = 1.89 \cdot 10^{-4}$ and $\mu_1 = 0.19$, $\mu_2 = 2.11 \cdot 10^{-3}$, $\mu_3 = 3.10 \cdot 10^{-4}$ respectively.

Subsequently, adequate phases (cf. Fig. 1) were applied to every component of the superposition with an electro-optic phase modulator (EOPM, EOspace). We would like to point out that the EOPM can also be used for phase randomization to eliminate coherence between subsequent rounds [41, 42]. All of the modulators support 40 GHz of usable analog bandwidth. The radio-frequency (RF) driving signals were generated with a fast arbitrary waveform generator (AWG, Keysight, M1896A) providing a sampling rate of up to 92.16 GSa/s and 35 GHz of analog bandwidth. The full-width at half maximum (FWHM) duration of a one-bit signal was therefore ~ 12 ps. The phase factors were adjusted using the EOPM by programming four driving voltage signals consisting of approximately 150-ps-wide rectangular pulses (Fig. 1a) such, that their amplitudes corresponded

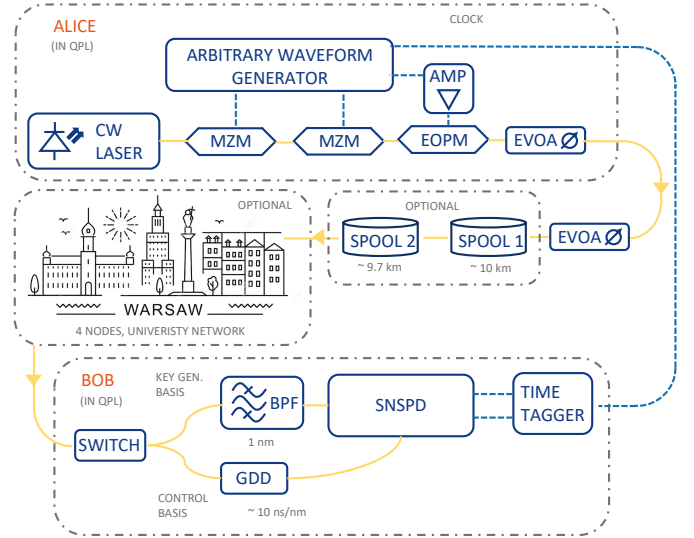


Fig. 2. Schematic of the key components of the experimental setup. A continuous wave (CW) laser is modulated with a Mach-Zehnder modulator (MZM) and phase modulator (EOPM) to generate optical pulses forming superpositions used as signals and decoy states. The optical signals are attenuated to a single photon level with a variable attenuator (EVOA). Attenuation of the quantum channel is controlled with another EVOA. Two spools of optical fiber (spool 1 and spool 2) were added to simulate propagation over a real link. Alternatively, the quantum channel comprised dark fibers deployed in the University of Warsaw urban fiber network, allowing measurements over certain fixed distances (see Fig. 3) by making a fiber loop. The signals impinge on a switch which we use to further detect either directly in the key generation basis (Z basis) or control basis (X basis). In the Z basis the signals are detected by time correlated single photon counting. In the X basis, by means of the temporal Talbot effect performed with the dispersion compensating module (DCM) providing group delay dispersion (GDD). Both Alice and Bob were placed in the Quantum Photonics Laboratory (QPL) at the Faculty of Physics, University of Warsaw. Yellow lines represent optical fiber connections and dashed blue lines depict RF cables.

to fractions or multiples of the phase modulator half-wave voltage (V_π). 3 samples of AWG memory were used to generate a single optical pulse. The RF signals driving the EOPM were also amplified with a high-bandwidth amplifier (RFLambda RFLUPA01G31GHz). The AWG also served as a source of the 10 MHz clock (CLK) signal distributed over an electrical cable to Bob. Finally, weak coherent states were generated by attenuating optical symbols to the single-photon level with an electronic variable optical attenuator (EVOA, Thorlabs, EVOA1550F).

To demonstrate the feasibility of our approach, we used a pre-programmed random sequence of symbols occupying 510720 samples of our AWG's memory. We then transmitted the sequence for 1 minute at every μ level, for different quantum channel attenuations. For the in-laboratory measurements the attenuation was set with another EVOA up to 20 dB. For convenience, the measurements were performed with a beam splitter that distributes signal to two detectors, effectively adding 3 dB of attenuation. On top of that we added two approximately 10-km-long spools of single-mode fiber to simulate a real link,



Fig. 3. Locations of the nodes of the dark fiber network of the University of Warsaw, overlaid on an Open Street Map of central Warsaw. Due to the network’s architecture the signals were routed over a 13-km-long fiber link via the University’s southern campus from node 2 to 3. Node 4 is located at a Historic Site of the European Physical Society (EPS).

which added 4.24 dB attenuation (including the insertion loss of the EVOA). To further demonstrate the feasibility we performed measurements over deployed dark fiber infrastructure (cf. Fig. 3) by making a fiber loop reaching the desired destination and reflecting the signal back to the Quantum Photonics Laboratory. We acquired data for every available node with and without the two fiber spools. We manually switched the measurement basis on the receiver side. Niobium-nitride superconducting nanowire single-photon detectors were used for time-domain measurements (SNSPDs, Single Quantum). Detector efficiency was equal to 84% according to the calibration data provided by manufacturer. Detection events were registered with a time-to-digital converter set to 1-ps-wide bins (Swabian Instruments, Time Tagger Ultra). The SNSPDs exhibited the jitter of 5 ps root mean square RMS and the time tagger of 10 ps. Thus, the Bob’s resultant jitter was 11 ps RMS. To measure in the control basis, the photons were additionally transmitted through a chirped-fiber-Bragg-grating-based dispersion compensating module (DCM), resulting in dispersive temporal broadening of the pulses. The measured insertion loss of the DCM was equal to 2.67 dB, and constituted the main contribution to the detection loss in the X basis. The contribution of other sources of optical loss was below 0.2 dB, primarily due to fiber connector losses. The DCM provided group delay dispersion (GDD) of 12900 ps² equivalent to 562 km of SMF-28 fiber. This amount of dispersion enabled observing the temporal Talbot effect [21], which we used to distinguish superpositions of the optical signals with different phases. The DCM also acted like a bandpass filter transmitting wavelengths in range 1558–1562 nm. To suppress the noise originating from the fiber network, we added an additional bandpass spectral filter (Haphit FPBP, 1 nm BW) in the Z basis.

4. RESULTS

In Fig. 4 we show the measured histograms of symbols from the temporal key-generation basis Z used in the experimental realization of the high-dimensional BB84 protocol. The symbols were 70 ps wide and separated by 279 ps, as expected. The separation between the pulses meets the condition given by Eq. 3 for the GDD of the dispersion compensating module and allows distinguishing the X -basis symbols using the temporal Talbot effect. The interference fringes overlap, resulting in imperfect distinction and in an increased QBER. This is the fundamental limit of our method, and the QBER value is strongly dependent on the detector timing jitter [21]. In Fig. 5a) we present results of a numerical simulation of X -basis QBER values for a range of detection timing jitter values, and for range of dimensions. Regardless of the relatively high QBER values in the X basis, we can still obtain positive key rates using the high-dimensional BB84 security proof [7]. We use this key rate formula for the analysis further throughout this section.

We employed Eq. 4 to simulate the key rates, using experimentally obtained parameters. We present simulated key rate (SKR) values for different jitters and corresponding X -basis QBERs in Fig. 5b). The Z -basis QBERs were experimentally measured for two and four-dimensional symbols and were always lower than 0.5%. This value is independent of the dimension due to the nature of time-bin encoding and was assumed for all dimensions for the simulation. With a larger alphabet we send more bits of information, but we also witness higher error rates in the control basis as a result of the overlap of the probability density functions. That trade-off constitutes the limitation, which would further be altered by different values of the detection jitter. In our scenario four and eight-dimensional states yield the highest key rate, and provide significantly better performances than qubits.

In Fig. 6 we show experimentally obtained key rates for qubits and ququarts using Eq. 4 in the case of in-laboratory measurements and measurements over the dark fiber network. The ququart clearly outperforms the qubit in both the cases.

5. SECURITY DISCUSSION

In the remaining part of the paper we would like to highlight potential security issues pertaining to our setup, and to QKD setups in general, related to basis-dependent detection probabilities. We will discuss our setup in this context and provide an analysis based on new theoretical developments.

Many QKD protocols allow dropping a measurement round if the receiving side did not register a click in any basis. The standard decoy-BB84 d -dimensional protocol security proof used in this work is one of them, but it assumes that, for any incoming state, the probability of accepting the round is the same for both the measurement bases. That is, the positive operator-valued measure (POVM) elements of the measurements in the X and Z bases corresponding to the rejection of a round are identical.

In our setup, the detectors of the two bases have different efficiencies and, additionally, in the X basis we have an additional insertion loss of the dispersion compensating module. This violates the assumption of the basis-independent detection efficiency required by standard security proof [38], but it could be fixed by inserting an additional attenuator in the Z basis. In the case of the proof-of-principle data presented in Fig. 6, the attenuation was applied in post-processing. In general, a detection efficiency mismatch may stem from using one or more delay line interferometers or modulators in one of the measurement bases,

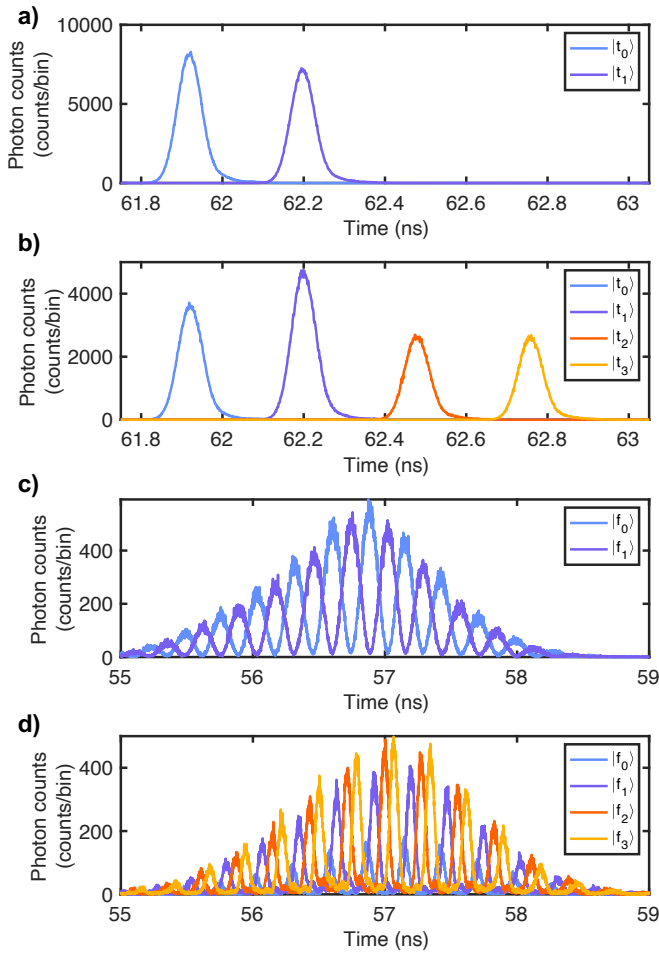


Fig. 4. Histograms of two and four-dimensional quantum states used in the QKD experiment measured for the infrastructure node no. 4 at ul. Hoža 69. The states were generated in the pseudo-random order, and the resultant sequence was transmitted for a minute. a) Z-basis symbols used for the two-dimensional encoding, Z-basis measurement; b) Z-basis symbols used for the four-dimensional temporal encoding, Z-basis measurement; c) X-basis symbols used for the two-dimensional encoding, X-basis measurement; d) X-basis symbols used for the four-dimensional encoding, X-basis measurement.

different efficiencies or qualities of the single-photon detectors, as well as from their varying dark count rate.

However, asymmetric detection efficiencies can also be mode-dependent. For example, single-photon detectors may have different efficiencies depending on the wavelength of the signal. In some protocols this may be resolved by sufficiently narrow spectral filters placed before the detectors. Yet, even if the detectors in both the bases in the setup described in section 3 were identical, the time-frequency mode dependence of the measurements is more subtle. The dispersion compensating module introduces wavelength-dependent delays, mixing the time and wavelength dependence of the measurement. This vulnerability is not specific for our setup, but is common for spectro-temporal implementations [14, 15, 43].

Such delays could map the signal outside the detection window of the following detector, thereby decreasing the X basis

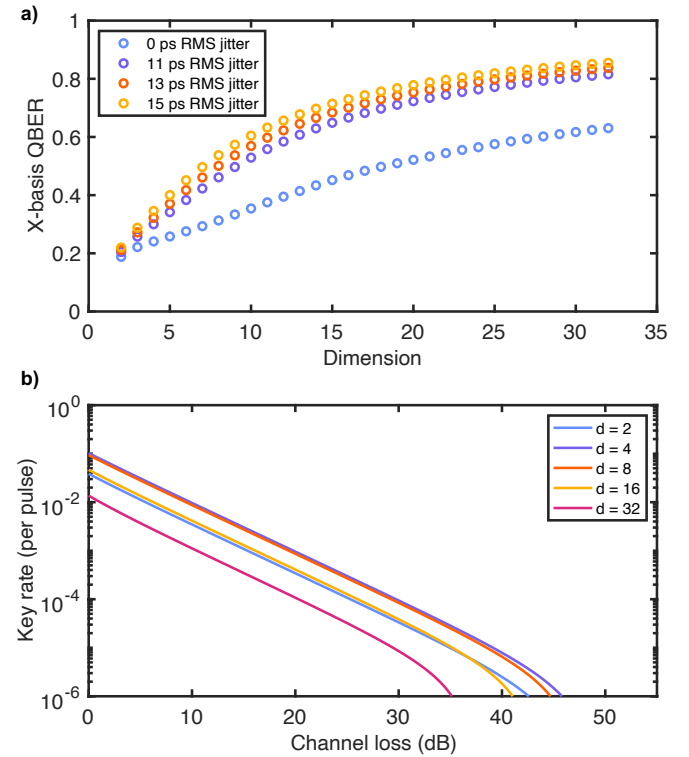


Fig. 5. X-basis QBER and corresponding SKR values for different dimensions. a) X-basis QBER values simulated for different values of jitter and dimensions of encoding. b) Simulated theoretically achievable key rate values as a function of channel loss for symbols of different dimensions, considering 15 ps RMS detection jitter.

detection efficiency compared to the Z basis. Likewise, tailored pulses generating a fixed outcome in the X basis could partially fall outside the Z basis time window, generating asymmetric detection efficiencies. Discrepancies between mathematical security proofs and experimental implementations may lead to successful quantum hacking attacks, and are often present in real implementations. For instance, a novel attack on BB84 protocols using asymmetric detectors is discussed in [38].

It is not possible to ensure that the detection probability in both bases is perfectly equal and mode-independent in real QKD systems. Indeed, deviations smaller than measurement errors in device characterizations could in principle be used by an attacker. Inclusion of such discrepancies in a security proof of a protocol strengthens the security of the real system. Here we will discuss, in an experimental context, a recently proposed global approach to tackling the basis detection efficiency mismatch issue.

6. TUNABLE BEAM SPLITTER PROTOCOL

An analytical security proof dropping the assumption on equal detection efficiency of the two bases is presented in Ref. [38]. The protocol assumes using a tunable beam splitter (TBS) on Bob's side – a device that allows rapidly switching between measurement bases. In the protocol this is a realistic device with a finite switching contrast, where maximal and minimal transmission are noted as η_{\downarrow} , η_{\uparrow} , and η_2 is an intermediate state. The TBS is capable of switching its transmission from value η_j to η_i and

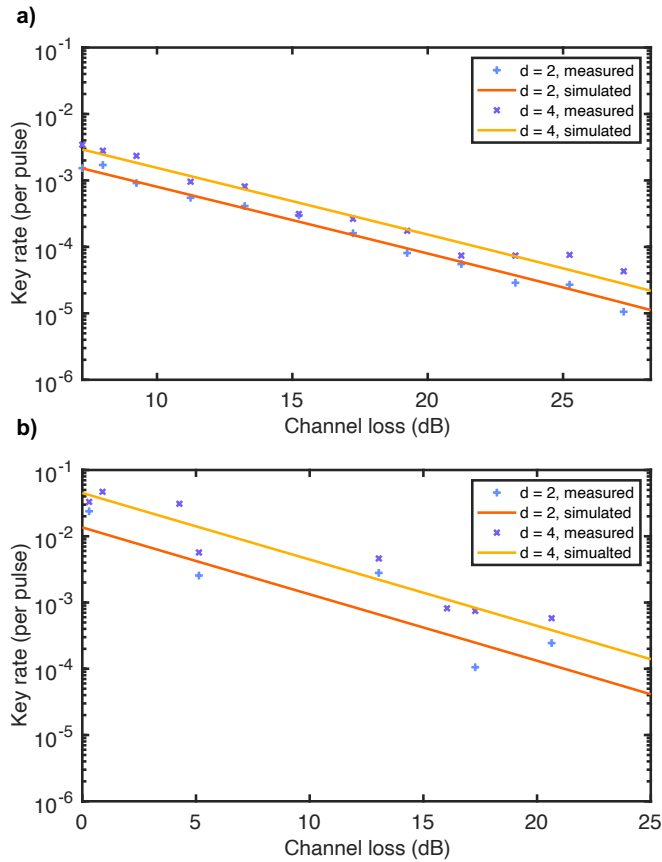


Fig. 6. Experimentally obtained key rates per pulse for two and four-dimensional encoding a) In-laboratory measurements including the two optional fiber spools. b) Measurements over dark fiber infrastructure with and without the two fiber spools.

back to η_j , where the time interval in which the transmission is equal to η_i coincides with the Z basis time window. For the security proof to follow, some assumptions on the three possible transmissions need to be satisfied:

$$\eta_{\uparrow} > \frac{\eta_{\downarrow}}{1 - \eta_{\downarrow}}, \quad (6)$$

$$\frac{\eta_X}{\eta_Z} > (\eta_{\downarrow})^{-1} \left(1 - \sqrt{1 - \frac{\eta_{\downarrow}}{\eta_{\uparrow}}} \right), \quad (7)$$

$$\eta_{\downarrow} < \eta_2 < \eta_{\uparrow}. \quad (8)$$

In our analysis we use a close-to-optimal choice of the intermediate transmission: $\eta_2 = (1/4)(\sqrt{\eta_{\downarrow}} + \sqrt{\eta_{\uparrow}})^2$. The TBS could be implemented for example with a double output Mach-Zehnder modulator (MZM) [43]. This kind of MZM is also available within generic photonic integrated technology, and was used to match detection efficiencies [44].

The resultant key rate can be obtained with the aforementioned Eq. (4) by applying expressions for phase error rate, yields, QBERs, and gains described in [38]. One of the main outcomes of the security proof of [38] is the derivation of the phase error rate upper bound, which is obtained without the usual assumption on equal detection efficiencies in the two bases. In Fig. 8 we present simulated key rate values for 0.5 dB and

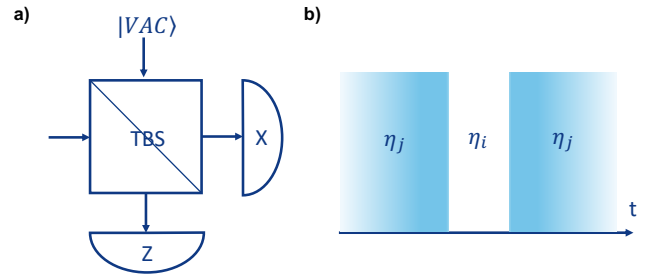


Fig. 7. Tunable beam splitter (TBS). a) Schematic of a tunable beam splitter used on Bob's side. The incoming signal is split and detected either in the X or the Z basis. b) Transmission of the TBS is set to a value η_i inside the window where the prepared symbol is expected, and to a value η_j outside of that interval.

0.1 dB measurement basis efficiency imbalance. The resultant key rate values are very sensitive to the efficiency imbalance and to the jitter due to the properties of our detection method. For our set of experimental parameters the resulting key rate would be negative, which shows how dangerous the efficiency mismatch can be. Negative values mostly stem from high attenuation difference caused by the DCM and technical limitations of our sender (Alice). The problem of imbalance can be effectively mitigated by adding an attenuator to one of the measurement bases in order to equalize the efficiencies. Attenuators with 0.1 dB accuracy are easily available and precise matching can be achieved with an EVOA, which makes this a convenient and cost-efficient fix. This shows that the more rigorous proof [38] will produce positive key rates with the appropriate modifications of the setup.

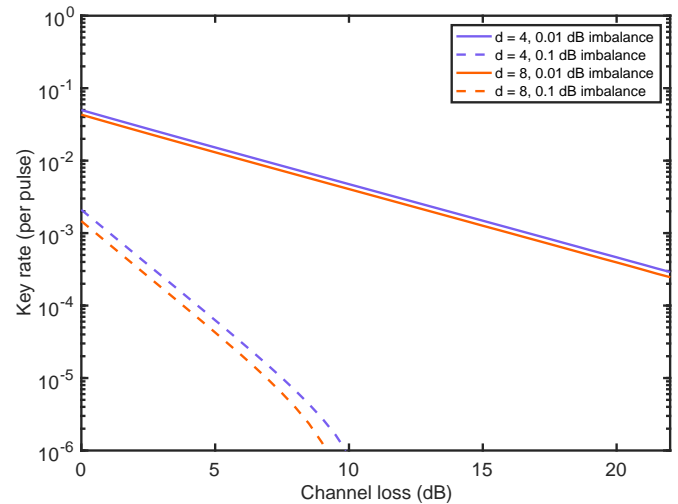


Fig. 8. Simulated key rate per pulse values considering 0.1 dB and 0.01 dB efficiency mismatch obtained according to the security proof provided in [38]. Key rate values were optimized over all μ values.

7. CONCLUSION

In summary, we demonstrate a high-dimensional BB84 QKD protocol with two and four-dimensional symbols in an all-fiber

setup using one single-photon detector per measurement basis. We successfully employ the temporal Talbot effect to detect high-dimensional phase-encoded superpositions by mapping frequency to time. We obtain positive key rates using the standard HD BB84 security proof in spite of the relatively high QBER, which is stemming from the overlap of the probability distributions and is strongly dependent on the detection timing jitter. We provide a comparison of theoretically-achievable key rates for a variety of dimensions based on a simulation with experimentally-obtained parameters. We show how basis efficiency mismatch and the security proof can severely impact the resultant key rate. We show vastly different key rates where differences stemmed from the considerations of the potential eavesdropper attacks within the security-proof framework. Our method is limited by low (sub-gigahertz) repetition rates, and the fact that the resultant shape of the superposition in the X basis occupies numerous time bins. Our measurement setup is prone to mode-induced detection efficiency mismatches, which can be accounted for by the security proof developed in [38], in combination with introduction of a tunable beam splitter and optical attenuators at the receiver side. In this regard, optical attenuators are easily obtainable, and tunable beam splitters can be realized as double output MZMs. Given the properties of the temporal Talbot effect, either the symbol separation can be digitally adjusted with respect to the dispersion of the quantum channel and receiver, or the GDD value at the receiver side can be selected to meet the requirements. This technique supports pulses of full width at half maximum (FWHM) of up to 100 ps, which makes using generically-available photonic integrated circuits (PICs) feasible for constructing transmitter modules [45]. Photonic integration of the receiver would require using on-chip GDD media and detectors, which is currently an emerging solution [46, 47]. In spite of that, PICs may enable integration and deployments due to available bandwidth, small form factor, cost-effectiveness, and the possibility of constructing double output MZMs [44]. Our proposal offers low complexity and high flexibility, which is crucial for quantum-photonic applications. Our findings may be an interesting consideration for constructing high-dimensional systems as well as deployment and development of qubit-based solutions, since the aforementioned basis efficiency mismatch problem is independent of the encoding dimension.

Funding. Federico Grasselli contributed to this work exclusively on behalf of Heinrich-Heine-Universität Düsseldorf (previous affiliation). A part of this work was supported by the QuICHE Project, which is supported by the National Science Center, Poland (project no. 2019/32/Z/ST2/00018) under QuantERA, which has received funding from the European Union's Horizon 2020 research and innovation programme under grant agreement no. 731473. Maciej Ogrodnik, Adam Widomski and Michał Karpiński appreciate funding from the University of Warsaw within the of the "Excellence Initiative — Research University" framework. Hermann Kampermann, Dagmar Bruß and Nikolai Wyderka acknowledge support by the QuantERA project QuICHE via the German Ministry of Education and Research (BMBF grant no. 16KIS1119K). Dagmar Bruß and Hermann Kampermann acknowledge support by the German Ministry of Education and Research through the project QuNET+ProQuake (BMBF grant no. 16KISQ137) and QuKuK (BMBF grant no. 16KIS1619). Giovanni Chesi and Chiara Macchiavello acknowledge the EU H2020 QuantERA ERANET Cofund in Quantum Technologies project QuICHE and support from the PNRR MUR Project PE0000023-NQSTI. Nathan Walk acknowledges funding from the BMBF (QPIC-1, Pho-Quant, QR.X).

Acknowledgments. We thank P. Rydlichowski and P. Celmer for assistance during the measurements using the fiber-optic infrastructure.

Disclosures. The authors declare no conflicts of interest.

Data availability. Data underlying the results presented in this paper can be obtained from the authors upon a reasonable request.

REFERENCES

1. S. Sajeed, P. Chaiwongkhot, A. Huang, H. Qin, V. Egorov, A. Kozubov, A. Gaidash, V. Chistiakov, A. Vasiliev, A. Gleim, and V. Makarov, "An approach for security evaluation and certification of a complete quantum communication system," *Sci. Reports* **11**, 5110 (2021).
2. F. Grünenfelder, A. Boaron, G. V. Resta, M. Perrenoud, D. Rusca, C. Barreiro, R. Houlmann, R. Sax, L. Stasi, S. El-Khoury, E. Hänggi, N. Bosshard, F. Bussi eres, and H. Zbinden, "Fast single-photon detectors and real-time key distillation enable high secret-key-rate quantum key distribution systems," *Nat. Photonics* **17**, 422–426 (2023).
3. W. Li, L. Zhang, H. Tan, Y. Lu, S.-K. Liao, J. Huang, H. Li, Z. Wang, H.-K. Mao, B. Yan, Q. Li, Y. Liu, Q. Zhang, C.-Z. Peng, L. You, F. Xu, and J.-W. Pan, "High-rate quantum key distribution exceeding 110 mb/s–1," *Nat. Photonics* **17**, 416–421 (2023).
4. Z. Yuan, A. Plews, R. Takahashi, K. Doi, W. Tam, A. Sharpe, A. Dixon, E. Lavelle, J. Dynes, A. Murakami, M. Kujiraoka, M. Lucamarini, Y. Tanizawa, H. Sato, and A. J. Shields, "10-mb/s quantum key distribution," *J. Light. Technol.* **36**, 3427–3433 (2018).
5. I. Vagniluca, B. Da Lio, D. Rusca, D. Cozzolino, Y. Ding, H. Zbinden, A. Zavatta, L. K. Oxenl owe, and D. Bacco, "Efficient time-bin encoding for practical high-dimensional quantum key distribution," *Phys. Rev. Appl.* **14**, 014051 (2020).
6. N. J. Cerf, M. Bourennane, A. Karlsson, and N. Gisin, "Security of quantum key distribution using d-level systems," *Phys. Rev. Lett.* **88**, 127902 (2002).
7. L. Sheridan and V. Scarani, "Security proof for quantum key distribution using qudit systems," *Phys. Rev. A* **82**, 030301 (2010).
8. N. T. Islam, C. C. W. Lim, C. Cahall, J. Kim, and D. J. Gauthier, "Provably secure and high-rate quantum key distribution with time-bin qudits," *Sci. Adv.* **3**, e1701491 (2017).
9. D. Cozzolino, B. Da Lio, D. Bacco, and L. K. Oxenl owe, "High-dimensional quantum communication: Benefits, progress, and future challenges," *Adv. Quantum Technol.* **2**, 1900038 (2019).
10. M. Kues, C. Reimer, P. Roztocky, L. R. Cort es, S. Sciara, B. Wetzel, Y. Zhang, A. Cino, S. T. Chu, B. E. Little, D. J. Moss, L. Caspani, J. Aza a, and R. Morandotti, "On-chip generation of high-dimensional entangled quantum states and their coherent control," *Nature* **546**, 622–626 (2017).
11. M. Mirhosseini, O. S. Maga a-Loaiza, M. N. O'Sullivan, B. Rodenburg, M. Malik, M. P. Lavery, M. J. Padgett, D. J. Gauthier, and R. W. Boyd, "High-dimensional quantum cryptography with twisted light," *New J. Phys.* **17**, 033033 (2015).
12. D. Cozzolino, D. Bacco, B. Da Lio, K. Ingerslev, Y. Ding, K. Dalgaard, P. Kristensen, M. Galili, K. Rottwitz, S. Ramachandran *et al.*, "Orbital angular momentum states enabling fiber-based high-dimensional quantum communication," *Phys. Rev. Appl.* **11**, 064058 (2019).
13. F.-X. Wang, W. Chen, Z.-Q. Yin, S. Wang, G.-C. Guo, and Z.-F. Han, "Characterizing high-quality high-dimensional quantum key distribution by state mapping between different degrees of freedom," *Phys. Rev. Appl.* **11**, 024070 (2019).
14. T. Zhong, H. Zhou, R. D. Horansky, C. Lee, V. B. Verma, A. E. Lita, A. Restelli, J. C. Bienfang, R. P. Mirin, T. Gerrits, S. W. Nam, F. Marsili, M. D. Shaw, Z. Zhang, L. Wang, D. Englund, G. W. Wornell, J. H. Shapiro, and F. N. C. Wong, "Photon-efficient quantum key distribution using time–energy entanglement with high-dimensional encoding," *New J. Phys.* **17**, 022002 (2015).
15. C. Lee, D. Bunandar, Z. Zhang, G. R. Steinbrecher, P. B. Dixon, F. N. C. Wong, J. H. Shapiro, S. A. Hamilton, and D. Englund, "Large-alphabet encoding for higher-rate quantum key distribution," *Opt. Express* **27**, 17539–17549 (2019).
16. F. Steinlechner, S. Ecker, M. Fink, B. Liu, J. Bavaresco, M. Huber, T. Scheidl, and R. Ursin, "Distribution of high-dimensional entanglement via an intra-city free-space link," *Nat. communications* **8**, 1–7 (2017).
17. F. Xu, X. Ma, Q. Zhang, H.-K. Lo, and J.-W. Pan, "Secure quantum key distribution with realistic devices," *Rev. Mod. Phys.* **92**, 025002 (2020).
18. J. D. Franson, "Bell inequality for position and time," *Phys. Rev. Lett.* **62**, 2205 (1989).
19. N. T. Islam, C. Cahall, A. Aragoneses, A. Lezama, J. Kim, and D. J.

- Gauthier, "Robust and stable delay interferometers with application to d -dimensional time-frequency quantum key distribution," *Phys. Rev. Appl.* **7**, 044010 (2017).
20. T. Brougham, S. M. Barnett, K. T. McCusker, P. G. Kwiat, and D. J. Gauthier, "Security of high-dimensional quantum key distribution protocols using Franson interferometers," *J. Phys. B* **46**, 104010 (2013).
 21. A. Widomski, M. Ogrodnik, and M. Karpiński, "Efficient detection of multidimensional single-photon time-bin superpositions," *Optica* **11**, 926–931 (2024).
 22. F. Vedovato, C. Agnesi, M. Tomasin, M. Avesani, J.-A. Larsson, G. Vallone, and P. Villorosi, "Postselection-loophole-free bell violation with genuine time-bin entanglement," *Phys. Rev. Lett.* **121**, 190401 (2018).
 23. H. F. Chau, W. Chen, C. Wang, G.-C. Guo, and Z.-F. Han, "Proof-of-principle experimental realization of a qubit-like qudit-based quantum key distribution scheme," *Quantum Sci. Technol.* **3**, 025006 (2018).
 24. A. Eckstein, B. Brecht, and C. Silberhorn, "A quantum pulse gate based on spectrally engineered sum frequency generation," *Opt. Express* **19**, 13770–13778 (2011).
 25. D. V. Reddy and M. G. Raymer, "High-selectivity quantum pulse gating of photonic temporal modes using all-optical Ramsey interferometry," *Optica* **5**, 423–428 (2018).
 26. L. Serino, J. Gil-Lopez, M. Stefszky, R. Ricken, C. Eigner, B. Brecht, and C. Silberhorn, "Realization of a multi-output quantum pulse gate for decoding high-dimensional temporal modes of single-photon states," *PRX Quantum* **4**, 020306 (2023).
 27. J. Ashby, V. Thiel, M. Allgaier, P. d'Ornellas, A. O. C. Davis, and B. J. Smith, "Temporal mode transformations by sequential time and frequency phase modulation for applications in quantum information science," *Opt. Express* **28**, 38376–38389 (2020).
 28. C. Joshi, B. M. Sparkes, A. Farsi, T. Gerrits, V. Verma, S. Ramelow, S. W. Nam, and A. L. Gaeta, "Picosecond-resolution single-photon time lens for temporal mode quantum processing," *Optica* **9**, 364–373 (2022).
 29. M. Karpiński, A. O. C. Davis, F. Sońnicki, V. Thiel, and B. J. Smith, "Control and measurement of quantum light pulses for quantum information science and technology," *Adv. Quantum Technol.* **4**, 2000150 (2021).
 30. M. K. Bochkov and A. S. Trushechkin, "Security of quantum key distribution with detection-efficiency mismatch in the single-photon case: Tight bounds," *Phys. Rev. A* **99**, 032308 (2019).
 31. A. Trushechkin, "Security of quantum key distribution with detection-efficiency mismatch in the multiphoton case," *Quantum* **6**, 771 (2022).
 32. Y. Zhang and N. Lütkenhaus, "Entanglement verification with detection-efficiency mismatch," *Phys. Rev. A* **95**, 042319 (2017).
 33. C.-H. F. Fung, K. Tamaki, B. Qi, H.-K. Lo, and X. Ma, "Security proof of quantum key distribution with detection efficiency mismatch," *Quantum Info. Comput.* **9**, 131–165 (2009).
 34. L. Lydersen and J. Skaar, "Security of quantum key distribution with bit and basis dependent detector flaws," *Quantum Info. Comput.* **10**, 60–76 (2010).
 35. J. Ma, Y. Zhou, X. Yuan, and X. Ma, "Operational interpretation of coherence in quantum key distribution," *Phys. Rev. A* **99**, 062325 (2019).
 36. H. F. Talbot, "Facts relating to optical science. No. IV," *Philos. Mag.* **9**, 401–407 (1836).
 37. T. Jansson and J. Jansson, "Temporal self-imaging effect in single-mode fibers," *J. Opt. Soc. Am.* **71**, 1373–1376 (1981).
 38. F. Grasselli, G. Chesni, N. Walk, H. Kampermann, A. Widomski, M. Ogrodnik, M. Karpiński, C. Macchiavello, D. Bruß, and N. Wyderka, "Quantum key distribution with basis-dependent detection probability," arXiv preprint, arXiv:2411.19874 (2024).
 39. S. Barnett, *Quantum information*, vol. 16 (Oxford University Press, 2009).
 40. F. Grasselli, *Quantum Cryptography* (SpringerCham, 2021).
 41. X.-B. Wang, "Beating the photon-number-splitting attack in practical quantum cryptography," *Phys. review letters* **94**, 230503 (2005).
 42. D. Rusca, A. Boaron, F. Grünenfelder, A. Martin, and H. Zbinden, "Finite-key analysis for the 1-decoy state qkd protocol," *Appl. Phys. Lett.* **112** (2018).
 43. M. Leifgen, R. Elschner, N. Perlot, C. Weinert, C. Schubert, and O. Benson, "Practical implementation and evaluation of a quantum-key-distribution scheme based on the time-frequency uncertainty," *Phys. Rev. A* **92**, 042311 (2015).
 44. P. Sibson, C. Erven, M. Godfrey, S. Miki, T. Yamashita, M. Fujiwara, M. Sasaki, H. Terai, M. G. Tanner, C. M. Natarajan *et al.*, "Chip-based quantum key distribution," *Nat. Commun.* **8**, 13984 (2017).
 45. A. Widomski, S. Stopiński, K. Anders, R. Piramidowicz, and M. Karpiński, "Precise on-chip spectral and temporal control of single-photon-level optical pulses," *J. Light. Technol.* pp. 1–8 (2023).
 46. M. Yu, D. Barton III, R. Cheng, C. Reimer, P. Kharel, L. He, L. Shao, D. Zhu, Y. Hu, H. R. Grant *et al.*, "Integrated femtosecond pulse generator on thin-film lithium niobate," *Nature* **612**, 252–258 (2022).
 47. A. Trenti, M. Achleitner, F. Prawits, B. Schrenk, H. Conradi, M. Kleinert, A. Incoronato, F. Zanetto, F. Zappa, I. D. Luch *et al.*, "On-chip quantum communication devices," *J. Light. Technol.* **40**, 7485–7497 (2022).